CT AND MRI FUSION FOR POSTIMPLANT PROSTATE BRACHYTHERAPY EVALUATION

Ehsan Dehghan[1*], *Yi Le*[2] , *Junghoon Lee*[2] , *Danny Song*[2] , *Jerry L. Prince*[2] , *Gabor Fichtinger*[3†]

[1] IBM Research, San Jose, CA, USA
[2] Johns Hopkins University, Baltimore, MD, USA
[3] Queen's University, Kingston, ON, Canada

ABSTRACT

Postoperative evaluation of prostate brachythrapy is typically performed using CT, which does not have sufficient soft tissue contrast for accurate anatomy delineation. MR-CT fusion enables more accurate localization of both anatomy and implanted radioactive seeds, and hence, improves the accuracy of postoperative dosimetry. We propose a method for automatic registration of MR and CT images without a need for manual initialization. Our registration method employs a point-to-volume registration scheme during which localized seeds in the CT images, produced by commercial treatment planning systems as part of the standard of care, are rigidly registered to preprocessed MRI images. We tested our algorithm on ten patient data sets and achieved an overall registration error of 1.6 ± 0.8 mm with a running time of less than 20s. With high registration accuracy and computational speed, and no need for manual intervention, our method has the potential to be employed in clinical applications.

Index Terms— Multi-Modality Registration, Prostate Brachytherapy, MRI, CT

1. INTRODUCTION

During postimplant dosimetry in low-dose-rate prostate brachytherapy (hereafter prostate brachytherapy), the delivered dose to the target gland and the organs at risk is quantitatively assessed. Precise localization of the implanted radioactive seeds and delineation of the relevant anatomical structures are necessary for an accurate postimplant dosimetry. Typically, postimplant dosimetry is performed using CT, which provides excellent seed visualization, but the prostatic anatomy is poorly differentiated [1]. The delineation of the prostate in CT is subjective and it adversely affects the accuracy of dosimetry [1]. In contrast, T2-weighted MR images provide the best available soft tissue visualization

[2]; however, seed localization in T2-weighted MR images is challenging [3, 4]. Fusion of MRI and CT can bring together the strengths of these complementary imaging modalities and provide accurate visualization of seeds and structural anatomy in a combined image. In fact, the American Association of Physicists in Medicine recommends that optimal imaging for postoperative brachytherapy dosimetry should include MRI [5].

Co-registration of CT and MR images of prostatic anatomy has been proposed previously, mainly by matching anatomical landmarks such as bones, bladder, and urethra [6, 7]. However, these methods cannot take into account the inevitable motion of the prostate with respect to the selected landmarks. Manually or semi-automatically localized seeds in MR and CT images were used as landmarks as well [8, 4]. Manual identification of matching seeds in MR and CT images is time-consuming and difficult. Mutual information has been employed for MR-CT fusion as well, but manual initialization—using landmarks or seed tracks—was necessary to provide accurate initial alignment [9, 2, 3].

In this paper, we propose an automatic method for CT-MR fusion with application in postimplant prostate brachytherapy dosimetry. Our method obviates the need for manual intervention to localize matching seeds or anatomical landmarks. Thus, it significantly simplifies brachytherapy postoperative dosimetry. In brachytherapy standard workflow, the implanted seeds are localized in CT by a commercial brachytherapy system and are used to calculate the dose. We take advantage of the availability of the seed positions and register the seeds from CT, as a point set, to the MR image volume. In our approach, during an image processing step, several filters are applied to the MR image volume to enhance the intensity profile of the seeds, which will in turn drive an intensity-based registration. Then, an evolutionary optimizer is used to maximize the overlap between the seeds, localized in CT and the processed MR volume by maximizing a point-to-volume similarity metric. Since this similarity metric quantifies the seed overlap between CT and MR volume only inside the prostate, the registration algorithm is not prone to yielding erroneous registration due to inevitable motion of the prostate with respect to bladder or pelvic bone.

We employ a similarity metric and optimizer previously

---

used by Dehghan *et al.* [10]. The salient feature of our registration approach lays in image processing step, where we apply a series of morphological filters, in order to enhance the visibility of seeds in the MR images.

In the following sections, we present the different components of our registration algorithm and prove its performance on clinical data. In particular, our registration results on ten patient data sets show excellent visual agreement between the seeds localized in CT, and MR image volume. Furthermore, the results of the automatic CT-MR registration are compared against manual registration as the ground truth.

2. METHODS

In current clinical practice, CT and MRI are acquired within a short time interval on day-1. The center points of seeds in the CT images are localized by the post-treatment analysis module of the clinical brachytherapy system and exported in standard DICOM-RT format. We register these seeds to the processed MR volume. Between CT and MR imaging, the structures inside the lower pelvis may move and deform, while shape and volume changes of the prostate gland are negligible, because: (1) Edematic growth or shrinkage and seed migration in such a short time interval and one day postimplant has not been observed. (2) We maintain a relaxed and identical supine body posture during CT and MRI imaging, which results in negligible deformation of the prostate as proven by extensive literature in prostate external beam radiotherapy. Seeds are implanted inside the entire prostate, so a registration of the seeds should assure a correct registration of the entire prostate gland, which is sufficient for subsequent dosimetric analysis. This explains why rigid registration of seeds implanted in the prostate gland serves our clinical purpose.

2.1. MR Image Processing

Our registration scheme maximizes the overlap between the seeds localized in CT (CT seeds) and the seed-like structures in the MR images. Therefore, we process the MR images in order to enhance the visibility of seeds in them.

As part of the normal clinical process, the prostate is delineated in the MR images for dosimetry calculations in the commercial brachytherapy planning system and contours are exported in DICOM-RT format. We use these contours to select the volume of interest (VOI) in the MR images, to limit the search region around the prostate gland, thereby increasing the likelihood of convergence to the global optimum. The VOI is selected, automatically, as a box that tightly encloses the prostate in all directions, such as shown in Fig.1(a).

Since the seeds appear as dark signal-voids in the MR images, we negate the image and apply a threshold to the negated image (see Fig. 1(b)). In this case:

$$I_{\mathrm{N}}(x,y,z) = \begin{cases} T_1 - I(x,y,z) & \text{if} \quad I(x,y,z) < T_1 \\ 0 & \text{if} \quad I(x,y,z) \geq T_1 \end{cases} \quad (1)$$

where $I(x,y,z)$ is the VOI, T_1 is the threshold value, and $I_{\mathrm{N}}(x,y,z)$ is the negated and thresholded image, x and y axes are along the horizontal and vertical axes of each slice and the z axis is perpendicular to the slice planes. The threshold value T_1 is the 90th percentile of intensity in image I. Note that this thresholding only saturates the background but does not detect the seeds. Then, we apply morphological image erosion using a disk structural element with radius r to fully cover the seed images ($r = 4$ pixels in this work) and produce an eroded image $I_{\mathrm{E}}(x,y,z)$ (Fig. 1(c)). Following that, we perform morphological image reconstruction to produce a reconstructed image $I_{\mathrm{R}}(x,y,z)$ (see Fig. 1(d)), using I_{E} as the marker image and $I_{\mathrm{N}} + 10$ as the mask image. Image erosion and reconstruction are applied slice by slice. Finally, $I_{\mathrm{S}}(x,y,z)$ is produced by subtraction of the reconstructed image I_{R} from the mask image. By adding a constant intensity to I_{N} and using it as the mask image, we allow the background in I_{E} to be dilated to match the intensity of the background of the mask image. Note that small and bright circular shapes (seed candidates) in the marker image were removed by erosion. Therefore, these regions cannot increase their intensity to match the intensity of the corresponding regions in the mask image, as the marker image stops evolving. Therefore, small and bright circular regions stand out in I_{S} (see Fig. 1(e)). We normalize I_{S} between 0 and 1. As it can be seen in Fig. 1(e), the image background is significantly suppressed and seed visualization is enhanced. However, there is some residual background in I_{S} that we try to remove by a second thresholding step. In this step, we produce the binary image $I_{\mathrm{T}}(x,y,z)$ by applying a binary threshold filter to $I_{\mathrm{S}}(x,y,z)$. The threshold value T_2 is the 99th percentile of image intensity of I_{S}. This binary image is labeled using the connected component labeling algorithm. The clusters that have a volume smaller than 10% of a seed are removed as false positives. Also, the cluster with the largest volume is removed as a candidate for the catheter present in the urethra.

Figure 1 shows the results of each step of the filtering process. Note that this process will not remove all the false positives. In addition, there are several missing seeds. However, our proposed registration method is robust to false positives and missing seeds because the optimizer hones in on seeds that are mutually present.

A binary image is not suitable for intensity-based registration as the image does not have a smooth intensity change to guide the optimizer. To remedy this problem, we first apply a distance transform to each slice of $I_{\mathrm{T}}(x,y,z)$. The distance transform measures the distance of every pixel from the closest white pixel in the same slice. Finally, a blurred image $I_{\mathrm{G}}(x,y,z)$ (see Fig. 1(f)) is produced by application of a Gaussian function to the distance image. The Gaussian function has a zero mean and a standard deviation of σ. A large value for σ decreases the size of the basin of convergence. On the other hand a small σ increases the effects of false positives. In this work, σ is chosen such that the image intensity
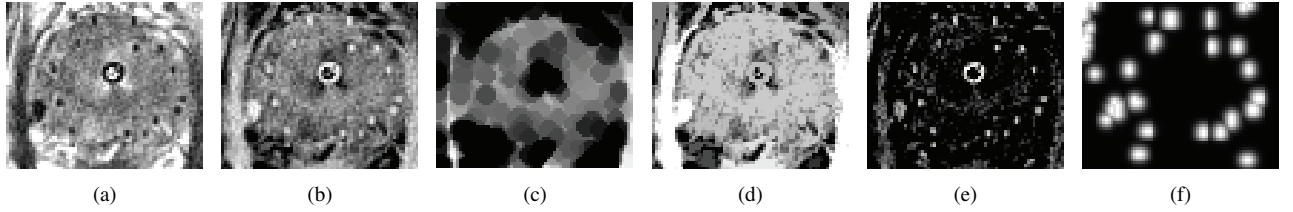
Fig. 1. MR image processing steps: (a) original slice (contrast changed for better visualization), (b) negated and thresholded slice, (c) eroded slice, (d) reconstructed slice, (e) the difference between the mask and the reconstructed images, (f) Gaussian blurred image. Note that the catheter in is removed in (f).

is equal to 0.75 at 1 mm away from a white pixel. This final image has a smooth intensity that can be used by the optimizer to hone in on the optimal value (see Fig. 1(f)).

2.2. Registration

As mentioned, deformation and seed motion is negligible due to the short time interval between CT and MR image acquisitions. Therefore, we use a rigid transformation $\mathbf{T}$ between the CT and MR coordinates. We calculate a point-to-volume similarity metric by integrating the processed MR image intensity inside cuboids V with dimensions $2 \times 2 \times 6$ mm^3 around each CT seed in the MR coordinate system. We have:

$$S = \sum_{k=1}^{N} \iiint_{V_k} I_\mathrm{G} \left(\mathbf{T}(s_k^{\mathrm{CT}}) + \begin{bmatrix} x \\ y \\ z \end{bmatrix} \right) dx\,dy\,dz, \quad (2)$$

where, S is the point-to-volume similarity metric, s_k^{CT} represents the coordinates of the kth seed in the CT coordinate system, and N is the number of implanted seeds.

We maximize this similarity metric using the Covariance Matrix Adaptation Evolutionary Strategy (CMA-ES) [11] which is a stochastic and gradient-free algorithm suitable for nonlinear and nonconvex problems. We employed nearest-neighbor interpolation to calculate the image intensity at non-grid points, and upsampled I_G along the z axis with a factor of 2 to reduce the effects of large slice spacing.

3. RESULTS AND DISCUSSION

We tested our registration on CT and MR images of ten patients, acquired within an approximately 1 hour time interval one day after the implant. Implanted seeds were ^{103}Pd seeds (Model 200, TheraSeeds, Theragenics, Buford, GA). MR images are T2-weighted (TE/TR = 104/5390 ms) acquired with a surface coil—without an endorectal coil—using a 1.5T Siemens MAGNETOM Espree device. The MR images have a slice thickness of 3 mm and in-plane pixel spacing of 0.52 to 0.94 mm. CT images have a slice thickness of 3 mm, acquired using a Philips Brilliance Big Bore CT scanner. A catheter was inside the patient's urethra during MR and CT scanning for better visualization of the urethra. A

board-certified medical physicist generated the ground truth registrations by manually registering the CT and MR images using seed locations and anatomical landmarks.

Our registration algorithm was initialized by coinciding the center of mass of the CT seeds with the center of the VOI. The rotation angles were initialized at zero. The search region was limited to ± 15 mm for translation parameters and $\pm 15°$ for rotation angles. This search region is sufficiently large for our application since 15 mm is at least 25% of the VOI, and the prostate has little rotation in supine position even due to changes in bladder and rectal fillings. Figure 2 shows the registration results, demonstrating excellent visual agreement between the seeds and signal-voids in the MR images.

The error vector was measured as the difference between the positions of each seed in the MR coordinate system, obtained using automatic and manual registrations. Table 1 shows the projection of the error vector along each axis and the overall error for each patient. The automatic registration shows an overall error of 1.6 ± 0.8 mm. Average error for seven out of ten patients is less than 2 mm. Note that errors of less than 2 mm are considered as clinically acceptable as their effect on the final dosimetry parameters is negligible [12]. The average error for three patients is slightly larger than 2 mm. The MR images of these three patients have the largest in-plane pixel spacing (0.94 mm) among our 10 patients. The large in-plane pixel spacing contributes to larger in-plane registration errors and hence, larger overall registration error.

We implemented our algorithm in MATLAB on a computer with a Core 2 CPU (2 GHz) and 2GB of RAM. The registration time was less than 20 s which is about 100 times shorter than the runtime of almost 30 min reported in [2, 9].

As mentioned, our registration method requires the CT seeds and prostate contours, both of which are required as part of the standard clinical workflow and are obtained from the commercial brachytherapy treatment analysis software. The results are inputted into our registration method which works fully automatically henceforth.

4. CONCLUSIONS

We presented an automatic image-based registration for fusion of MR and CT images of the prostate after brachyther-
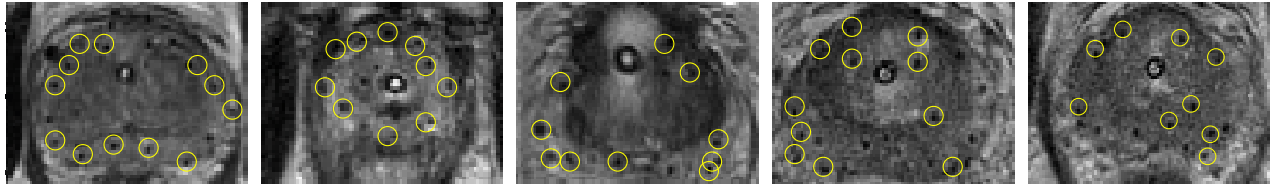
Fig. 2. Registered seeds overlaid on MR images of the prostate. The presented registered seeds are only one pixel long. Therefore, some seed-like voids in each slice may be associated with registered seeds in an adjacent slice that are not shown.

Table 1. Registration error for each patient

#	Abs. Proj. Error (mm) Mean±STD			Error
	x	y	z	(mm)
1	0.4 ± 0.3	0.8 ± 0.5	0.6 ± 0.4	1.2 ± 0.5
2	1.4 ± 0.4	1.6 ± 1.1	1.1 ± 0.7	2.6 ± 0.6
3	0.6 ± 0.3	1.9 ± 0.4	1.3 ± 0.4	2.5 ± 0.4
4	0.9 ± 0.7	1.2 ± 0.7	1.3 ± 0.9	2.2 ± 0.7
5	0.8 ± 0.5	0.4 ± 0.2	1.1 ± 0.8	1.5 ± 0.7
6	0.6 ± 0.1	0.2 ± 0.2	0.5 ± 0.3	0.8 ± 0.2
7	0.6 ± 0.4	0.9 ± 0.2	0.8 ± 0.5	1.5 ± 0.3
8	0.6 ± 0.4	0.6 ± 0.4	0.5 ± 0.2	1.1 ± 0.3
9	0.1 ± 0.1	1.0 ± 0.3	0.6 ± 0.4	1.2 ± 0.4
10	0.5 ± 0.3	0.3 ± 0.1	0.7 ± 0.5	1.0 ± 0.4
All	0.6 ± 0.5	0.9 ± 0.8	0.8 ± 0.6	1.6 ± 0.8

apy. Our method registers a set of seeds localized in CT to a processed MR volume. We achieved an average registration error of 1.6 mm for ten patients for which, the registration error was defined as the distance between the automatically and manually registered seeds. Our method showed consistently successful registration on ten patients, despite the diversity in the number of the implanted seeds (61–103) and MR image pixel spacing (0.52–0.94 mm). With small registration error and short computational time, our algorithm is promising as a practical solution for postoperative dosimetry in prostate brachytherapy. Validation on a larger cohort of patients is part of the future work.

5. REFERENCES

[1] B. H. Han *et al.*, "The effect of interobserver differences in post-implant prostate CT image interpretation on dosimetric parameters," *Med. Phys.*, vol. 30, pp. 1096–1102, 2003.

[2] P. L. Roberson *et al.*, "Use and uncertainties of mutual information for computed tomography/magnetic resonance (CT/MR) registration post permanent implant of the prostate," *Med. Phys.*, vol. 32, pp. 473–482, 2005.

[3] S. Vidakovic *et al.*, "Post-implant computed tomography-magnetic resonance prostate image registration using feature line parallelization and normalized mutual information," *J. Appl. Clin. Med. Phys.*, vol. 8, pp. 21–32, 2007.

[4] E. S. Kim, "Improved seed-based MR and CT image registration for prostate brachytherapy," M.S. thesis, Massachusetts Institute of Technology, 2004.

[5] R. Nath *et al.*, "AAPM recommendations on dose prescription and reporting methods for permanent interstitial brachytherapy for prostate cancer: Report of task group 137," *Med. Phys.*, vol. 36, no. 11, pp. 5310–5322, 2009.

[6] R. J. Amdur *et al.*, "Prostate seed implant quality assessment using MR and CT image fusion," *Int. J. Radiat. Oncol. Biol. Phys.*, vol. 43, no. 1, pp. 67 – 72, 1999.

[7] K. Kagawa *et al*, "Initial clinical assessment of CT-MRI image fusion software in localization of the prostate for 3D conformal radiation therapy," *Int. J. Radiat. Oncol. Biol. Phys.*, vol. 38, no. 2, pp. 319–325, 1997.

[8] D. Taussky *et al.*, "Sequential evaluation of prostate edema after permanent seed prostate brachytherapy using CT-MRI fusion," *Int. J. Radiat. Oncol. Biol. Phys.*, vol. 62, no. 4, pp. 974 – 980, 2005.

[9] P. W. McLaughlin *et al.*, "The use of mutual information in registration of CT and MRI datasets post permanent implant," *Brachytherapy*, vol. 3, pp. 61–70, 2004.

[10] E. Dehghan *et al.*, "Ultrasound–fluoroscopy registration for prostate brachytherapy dosimetry," *Med. Image Anal.*, vol. 16, no. 7, pp. 1347–1358, 2012.

[11] N. Hansen, "The CMA evolution strategy: a comparing review," in *Towards a new evolutionary computation. Advances on estimation of distribution algorithms*, vol. 192, pp. 75–102. Springer Berlin / Heidelberg, 2006.

[12] M. Wu and G. Fichtinger, "Effects of TRUS and fluoroscopy registration error on dosimetric quality in prostate brachtherapy," in *Int. Conf. Society for Medical Innovation and Technology (SMIT)*, 2010, vol. 19, p. 28.